Crystal Pattern Formation and Transitions of PEO Monolayers on Solid Substrates from Nonequilibrium to near Equilibrium

Xuemei Zhai, Wei Wang,* Guoliang Zhang, and Binglin He

The Key Laboratory of Functional Polymer Materials of Ministry of Education and Institute of Polymer Chemistry, College of Chemistry, Nankai University, Tianjin 300071, China

Received July 25, 2005; Revised Manuscript Received November 6, 2005

ABSTRACT: The crystal pattern formation and transition of the monolayers of a low-molecular-weight poly(ethylene oxide) ($\bar{M}_n$ = 5000 g/mol) on the surface of silicon wafer were studied using atomic force microscopy with a hot stage in the temperature range $25 \le T_c \le 59$ °C. Our observations show that the crystal patterns are greatly dependent on the crystallization temperature, T_c. At $25 \le T_c < 39$ °C a dendrite pattern with a fractal dimension $D_p = 1.672 \pm 0.027$ was found. At $39 < T_c \le 48$ °C the crystal pattern become seaweed with the same fractal dimension. The difference between dendrite and seaweed patterns can be quantitatively described by the angle between main and side branches. The dendrite-to-seaweed transition occurred at $T_c = 39$ °C. At $54 \le T_c \le 59$ °C the crystals had a square shape. A dramatic change occurred at the transition temperature from 49 to 52 °C. In this temperature range the crystal pattern alters from seaweed to compact structure and finally to the square shape of single crystals. The possible formation mechanisms are discussed in the text.

Introduction

In nonequilibrium condition crystal growths can causes complex patterns that are an important topic of condensed matter physics in the past decades.[1−24] Different patterns, such as dendrite, seaweed (or densely branched morphology), and compact structure, have been found in some experimental observations[2−12] and fully represented by computer simulations[10,13−24] mainly based on the diffusion-limited aggregation (DLA) mechanism[13] but in consideration of different boundary conditions, such as supercooling, anisotropy strength, diffusivity, surface tension, etc., to explore the formation mechanisms.[14−24] Recently, it has been found by computer simulations that there are transitions between different patterns, such as the dendrite-to-seaweed transition, when the boundary conditions vary continuously and the morphological diagrams have been recommended.[23,24] Very unfortunately, to our best knowledge, there is no report presenting the experimental confirmation published regarding the pattern transitions in crystal systems, yet.

Because of their long chain nature, crystallization and melting of linear macromolecules are highly complex processes in comparison with small molecules.[25−27] Under the supercooling condition macromolecules kinetically prefer to be folded several times to form folded-chain (FC) lamellar crystals of which thickness is normally less than the contour length of molecules. Normally, FC crystals further organize into spherulites or, sometimes, larger single crystals highly dependent on crystallization conditions and having different shapes or patterns. In 1964, Keith and Padden have reported their findings of lamellar crystals with branched pattern formed by FC crystals of an isotactic polypropylene (PP) in a matrix of an atactic PP.[28] Since then, similar patterns have been repeatedly found mainly in the thin film samples of some crystallinable polymers, and the DLA mechanism was used to explain the formation of such patterns.[29−34]

In this work, we would like to report our investigations of the crystal pattern formations of poly(ethylene oxide) (PEO) monolayers characterized using a hot-stage AFM. When crystallization was performed at different crystallization temperatures, T_c, or supercooling conditions, ΔT ($\Delta T = T_m^0 - T_c$ where T_m^0 is equilibrium melting temperature), different crystal patterns, such as dendrite and seaweed, compact structure, and single crystals with regular shape, were visualized. Our further analyses of the patterns demonstrate the transitions from dendrite to seaweed, to compact, and, finally, to square single crystals as a function of ΔT_c only. We will discuss the pattern formation and transition mechanisms based on the previous theoretical and experimental results.

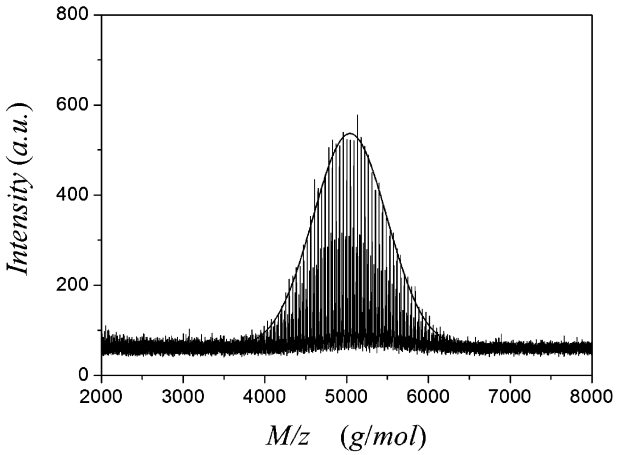

Figure 1. Molecular weight and its distribution of the PEO sample determined by Maldi-Tof mass spectrometry. The solid line is the fitting result using the Gaussian function. $\bar{M}_n$ = 5000 g/mol and σ = 454 g/mol.

Experimental Section

Materials. PEO used was purchased from Fluka. Its absolute molecular weight was precisely determined using a matrix-assisted laser desorption ionization time-of-flight (Maldi-Tof) mass spectrometer (Bruker Reflex II-TOF), as shown in Figure 1. The molecular weight distribution obeys a Gaussian distribution with $\bar{M}_n$ = 5000 g/mol and a standard deviation σ = 454 g/mol, so the precise polydispersity index is $\bar{M}_w/\bar{M}_n = 1 + (\sigma/\bar{M}_n)^2 = 1.008$. This

* To whom the correspondence should be addressed. E-mail: weiwang@nankai.edu.cn.

10.1021/ma051624y CCC: $33.50
Published on Web 12/07/2005

value is lower than the value ($\bar{M}_w/\bar{M}_n = 1.05$) measured using a gel permeation chrotomagraphy (GPC Waters) in *N*,*N*-dimethylformamide (DMF) solution and calibrated using PEO standards. This polymer contains a methyl group at one end and a hydroxyl group at other end. The maximum length of the molecules in the fully extended form is $L = l_m N = 31.6$ nm where the repeating unit length is $l_m = 0.2783$ nm,[35,36] and the degree of polymerization is $N = 114$. This PEO may form lamellae with a thickness, l, which is always an integer submultiple of the total chain length L as $l(n) = L/n + 1$, where n is the number of folds (quantized folding).[36] So, $l(0) = 31.6$ nm, $l(1) = 15.8$ nm, $l(2) = 10.5$ nm, $l(3) = 7.9$ nm, and $l(4) = 6.3$ nm.

Sample Preparation. The samples for AFM studies were prepared as follows: The toluene solutions with a concentration of 0.01−0.02 wt % were prepared in glassware. The silicon wafers were cleaned in an ultrasonic water bath and then in an acetone bath. The thin PEO films on the surface of the silicon wafers were prepared simply by dropping the polymer solution at room temperature. The samples were dried at normal atmosphere overnight and then were treated in a vacuum oven at room temperature for 12 h. A monolayer of lamellar crystals with fractal-like patterns formed on the surface of the silicon wafers.[34] The cast samples were first heated to 75 °C for 5 min to let the lamellar crystals to melt completely. When the recrystallization temperature was lower than 40 °C, the samples were cooled to the selected temperatures to let the polymer recrystallize for 12 h. When the recrystallization temperature was higher than 40 °C, the samples were at first treated at a relatively lower temperature, such as 35 °C, to allow the formation of some nucleuses and then reheated to the selected temperatures to further crystallize for 12 h. The formation of these nucleuses was confirmed using AFM.

Instruments. A hot-stage multimode atomic force microscope (Digital Instrumental Nanoscope IV) was used to visualize the pattern formation of PEO lamellar crystals. The temperature of the hot stage can be precisely controlled within ±0.1 °C. All measurements were performed in tapping mode. The temperature of the hot stage and the height determined were calibrated following the methods and using a standard sample provided by the manufacturer.

Data Analysis. The digital images obtained by AFM were further analyzed using image analysis software and an applied program which can be downloaded from the Web site of the National Institutes of Health. During our image analysis the 8-bit AFM images were first binarized into black−white images. In this work we used the dilation method[37] to determine the fractal dimension, D_p, of the crystals. Actually, we obtain a fractal dimension of the curve of which the definition is

$$N(r) \propto r^{-D_p} \tag{1}$$

where N is the number of segments that are needed to approximate the curve and r the length of segments. In Euclidean geometry $D_p = 1$.

Results and Discussion

Patterns and Transitions. It is well-known that the thickness of lamellar crystals of PEO is a function of crystallization temperature.[34−36] It is very interesting to present that the crystal patterns of PEO monolayers are also highly dependent on the crystallization temperature. Figure 2 shows the different patterns observed in the temperature range from 25 to 59 °C. These AFM images demonstrate a clear variation in crystal patterns from a typical dendrite (images a and b), to a seaweed (images e and f), to a compact structure (image h), and, finally, to single crystals with regular square shape (images j−l) when the crystallization temperature was gradually increased. The patterns in images c, d, g, and i show the "mixed" patterns appearing in the transition regions. To have an easy understanding of the growth direction of the crystals, some dotted lines were placed on the backbones of some main or side branches and the arrows were used to point out their growth direction in these images showing the dendrite or seaweed pattern. It is worth mentioning that different length scales were used to have a good representation.

Images a and b show a typical tip-stable dendrite pattern, which has been deeply studied,[1,2] obtained from the samples crystallized at 25 and 30 °C for 12 h, respectively. The angle between the main and side branches is 90°, indicating that the crystals grew with a strong anisotropy. In image a there are at least two dendrites grown from two origins. There is no existence of a normal relation between the branches belonging to the two dendrites. This is indicative of that the substrate surface structure does not cause the anisotropic growth. In other words, it is a typical feature of folded-chain lamellae having a preferential growth direction.

Images c and d present the crystal patterns observed from the samples crystallized at 37.5 and 40 °C for 12 h. With increasing the crystallization temperature, the patterns are somehow different from those shown in the previous two images. The angles between main and side branches can be either 90° or 45°. In other words, the growth direction of side branches selects either at the normal direction to form dendrite crystals or at the direction having a 45° angle to form seaweed crystals. The average width of branches becomes broad. In images e and f the pattern has become typical seaweed, and slitting tips can be seen, meaning that crystal growth misses anisotropy, so the angle is about 45°. The average width of branches was further broadened.

When the crystallization temperature further increased from 49 to 52 °C, the crystal pattern has a dramatic change, as clearly shown in images g and h. When the temperature increases with a step of 1 deg, the pattern will be altered greatly. At 49 °C the crystals still have a finger-like pattern with very wide branches. At 50 °C a hopper-like or compact pattern with four segments is formed. The periphery is no longer smooth but becomes sawtooth-like. At 52 °C the crystal shape is still irregular, but its periphery is completely sawtooth-like. This crystal appears to be formed randomly by many small square single crystals. The dramatic variation in crystal pattern implies a turnover of the mechanism controlling the pattern formation.

Beyond 52 °C the crystallization condition is becoming close to equilibrium, so the crystals become faceted with a regular square shape until 60 °C. Within this temperature range, so far, only square single crystals with a thickness of extended-chain length were found. In images i−l several crystals are shown. Normally, the probability for nucleation should be extremely low at such high temperatures. In our experiment, such faceted single crystals were frequently observed, and the results are reproducible. We believe that the following two factors could play a role in inducing the melted PEO molecules to nucleate and then to form the larger crystals. The first may be due to the nucleation seeds formed when the samples were crystallized at 35 °C, while the second may be due to the inducing effect of the AFM tips when scanning the studied frame.

Quantitative Description of Pattern Transitions. To have a quantitative description of the pattern transitions, the fractal dimension of the curve of the patterns, D_p, the angles between the main and side branches, θ, and the characteristic width of the branches, W, were determined. To have a good understanding of the supercooling effect, the equilibrium melting point of this polymer was actually determined in-situ using the hot-stage AFM through measuring the size change of extended-chain crystals as a function of temperature in a slow heating

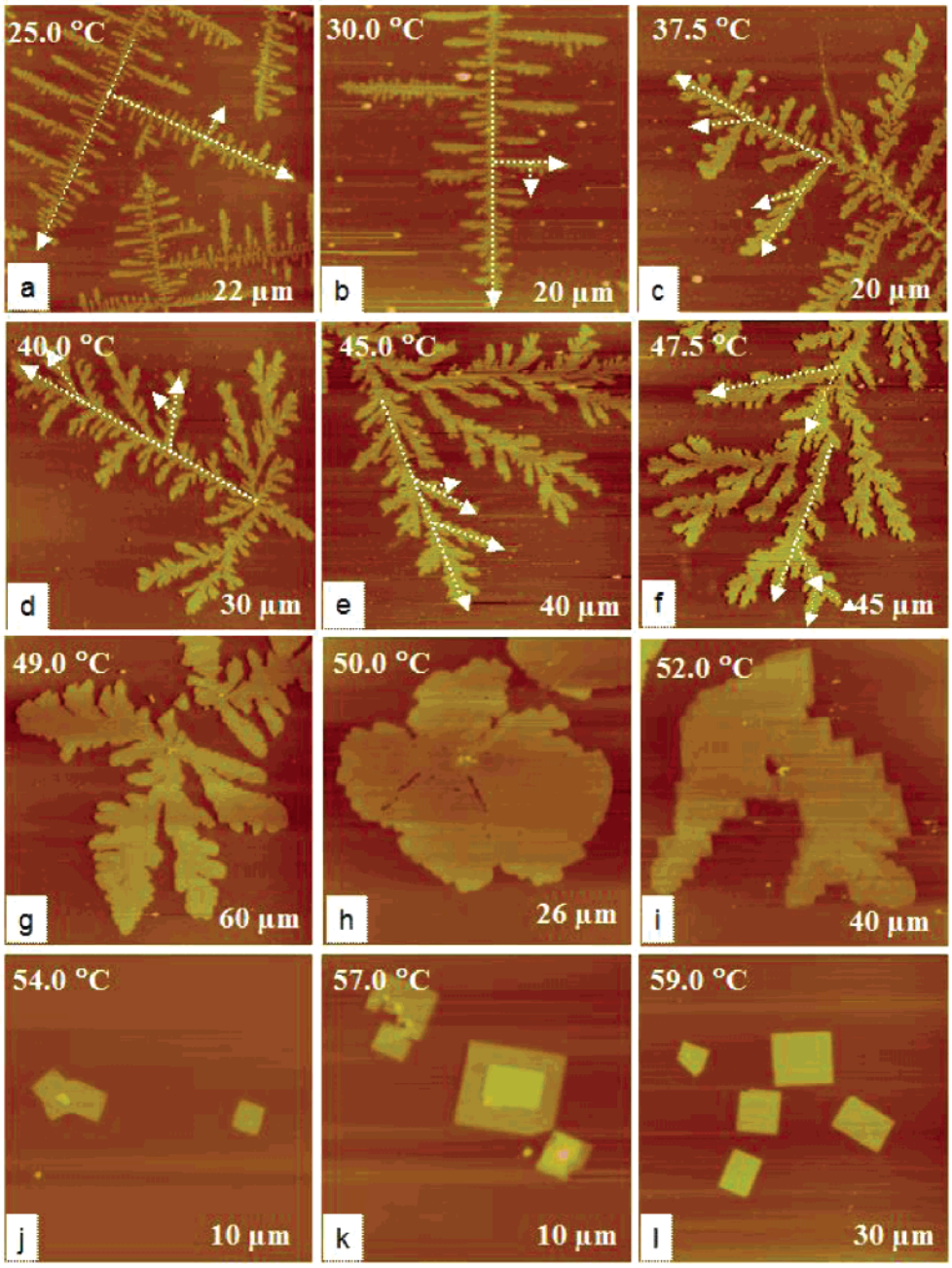

Figure 2. AFM height images showing the crystal patterns obtained at different crystallization temperatures. The height range is 60 nm for images a−c, 100 nm for images d−g, 150 nm for images h and i, and 300 nm for images j−l.

condition: 0.2 °C per 15 min. It is found that at 62.2 °C the crystals melted completely, so $T_m^0 \cong 62.2$ °C.

Figure 3 shows the plots D_p, θ, and W vs ΔT or T_c. It is very interesting to see their different temperature dependences. At $14.7 \leq \Delta T \leq 37.2$ °C (or $25 \leq T \leq 47.5$ °C) D_p has an average value of 1.672 ± 0.027 and W increases linearly. These are the indication of "fractality" of both the dendrite and seaweed patterns, also meaning that their formation is mainly controlled by underlying DLA mechanism.[13] The same fractal dimension for the dendrite and seaweed patterns in this temperature range makes us impossible to distinguish the pattern transition between dendrite and seaweed merely from the fractal dimension. However, at $20 \leq \Delta T \leq 27$ °C the θ value changes from 90° to 45°, correctly corresponding to the pattern transition as mentioned above. Therefore, it is a parameter that can describe the dendrite-to-seaweed transition correctly and quantitatively. The solid curve in the figure is the fitting result obtained using Boltzmann function $\theta = \theta_2 - (\theta_1 - \theta_2)/(1 + \exp((\Delta T - \Delta T_0)/w))$ with $\theta_1 = 44°$, $\theta_2 = 86°$, $\Delta T_0 = 23.1$ °C, and $w = 0.95$ °C. θ_1 and θ_2 are the angles between the main and side branches of seaweed and dendrite patterns, respectively. The dendrite-to-seaweed transition occurs at $T_0^{d\to s} = 39.1$ °C with a relatively narrow transition zone.

A dramatic reduction of D_p starts at $\Delta T = 13.2$ °C (or $T_c = 49$ °C). At the same time W value dramatically increases and then cannot be measured when the seaweed pattern no longer exists. When ΔT decreases from 13.2 to 12.2 °C (one degree only!), the D_p value reduces from 1.57 to 1.27, corresponding to a crystal pattern transition from seaweed to compact structure (images g and h in Figure 1). Lowering the fractal dimension is an indication of missing fractality, the typical feature of the compact patterns, further meaning that DLA mechanism is losing in controlling pattern formation. Further decreasing ΔT (or increasing T_c) the D_p value gradually reduces to 1.0 at

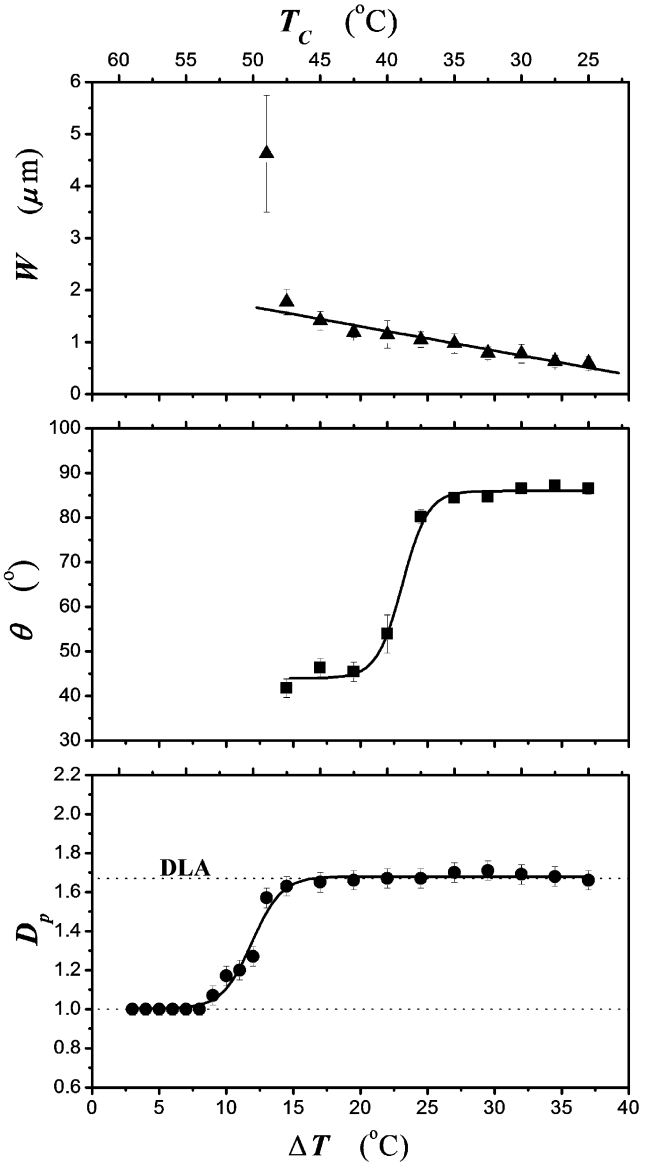

Figure 3. Plots of W, θ, and D_p vs ΔT (or T_c).

$\Delta T = 8.2$ °C (or $T_c = 54$ °C), showing that PEO molecules crystallize to form square single crystals with a thickness equal to the extended chain. The change of the fractal dimension can be also fitted using the Boltzmann function $D_p = D_{p2} - (D_{p1} - D_{p2})/(1 + \exp((\Delta T - \Delta T_0)/w))$, with $D_{p2} = 1.68$, $D_{p1} = 1.00$, $\Delta T_0 = 12.1$ °C, and $w = 1.11$ °C. $D_{p1} = 1.00$ means the fractal dimension of the square crystals formed at the crystallization condition near equilibrium. $\Delta T_0 = 12.1$ °C means that the transition from the fractal crystals to the square faceted crystals occurs at $T_0^{f\rightarrow fc} = 50.1$ °C, further implying that two kinds of mechanisms of controlling the pattern formation have equal contributions. At this temperature, the compact patterns were formed (see image h in Figure 2) and have the features of both the fractal and square crystals at different length scale.

Controlling Mechanisms. Clearly, the mechanism of controlling the pattern formation alters with decreasing ΔT. It is well-known that crystallization is a complex and kinetic-controlled process containing the following processes:[38] (1) the molecular diffusion process from the liquid phase to the interface, (2) the incorporation process of molecules into crystals at the interface between the crystal and liquid phases, i.e., a surface kinetic process, and finally (3) the diffusion process of latent heat at the interface. At different conditions one or couplings of these processes can be the key factor in governing the whole crystallization process, thus causing different patterns.

In the past decades a great number of theoretical studies that were carried out mainly through computer simulations[10,15−24] have indicated that process 1 is the major factor in determining the pattern formation of a crystallization process in nonequilibrium conditions, that is, the diffusion-controlling aggregation (DLA) mechanism.[13,14] The underlying DLA model can correctly describe the fractality of the crystal patterns, the most principal feature. This model is based on the assumption that sticking probability of the particles arriving at the surface of crystals is quite high (close to one), meaning that the particles (or molecules in this study) have no chance to select the correct sites to join the growing crystal front when they have arrived at the interfacial area between solid and liquid. The formation of different patterns attributes to the changes of boundary conditions related to the processes 2 and 3, which can affect the stacking probability more or less.[10,15−24] These boundary conditions can be supercooling (or crystallization temperature), anisotropic growth, heat diffusivity, surface tension, etc.

Normally, the fractal dendrite can be obtained by simulations using the noise-reduced DLA model with an emphasis on the effect of anisotropy.[18] The growth anisotropy may come from general microscopic anisotropy of the physical properties of the either systems self-or outside effects, like substrate directional growth due to anisotropic surface tension. Since there is no existence of a normal relation between the branches grown from different origins (see in image a in Figure 2), the substrate surface structure or, more exactly, anisotropic feature, like what has happened in using the lattice model to run simulations, does not cause the anisotropic growth. So, the anisotropy in our experiment comes from the directional crystallization of the lamellar crystals along a preferred growth direction.

The previous Monte Carlo simulations[20] of using a two-dimensional square lattice have shown that ramifying and seaweed-like patterns appears in the crossover domain between different preferred directions of dendrite growth, meaning in the case of particles missing their selective ability of joining to crystal sites. Therefore, the angles between main and side branches deviate from 90°. Our experimental results show $\theta = 45°$ for the seaweed pattern. This is because the sticking possibility of molecules on the growth front is affected. The simulations[16] have shown that the pattern would gradually change from ramifying to compact structure when the sticking possibility is gradually reduced from one to a very small value. At the same time, the fractal dimension, D_p, reduces to the value close to one. This alteration further means that DLA mechanism gradually loses its control in the pattern formation. The relaxation process to one of the nearest- or next-nearest-neighbor sites becomes the major mechanism of controlling the pattern formation of crystals after the molecules have moved to the crystal growth front and have been allowed to join the crystal. In this case the molecules will highly select the best position with the largest number of occupied nearest neighbor to join the crystal because the sticking probability becomes very low, so the potential energy becomes lowest. This also means that the nucleation and crystallization of molecules on the growth surface of crystals become the dominant step in determination of the crystal pattern.

In a narrow temperature range (about 5 °C), the governing mechanism will be altered. The pattern will have a dramatic change, as shown by the images g−i in Figure 2. At 49 °C, the

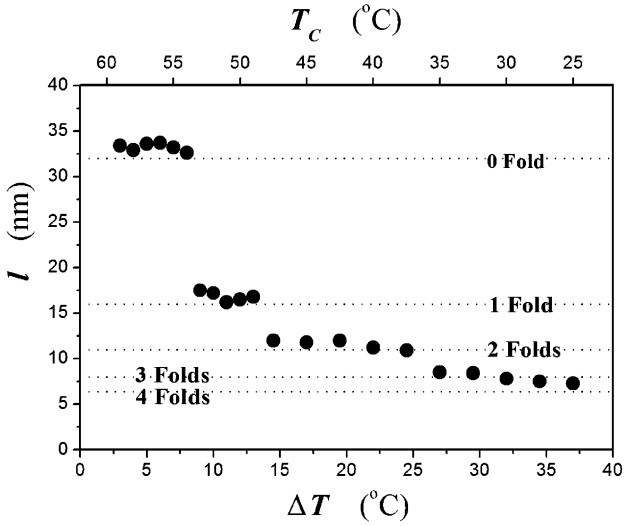

Figure 4. Plot of l vs ΔT or T_c showing a stepwise increase with increasing temperature.

DLA mechanism is still controlling the pattern formation to a certain extent, but at 52 °C the nucleation and crystallization of molecules on the growth surface of crystals is becoming the leading mechanism. The irregular shape of the crystal in image i in Figure 2 is attributed to the diffusion process controlling the macroscopic shape, while the sawtooth-like periphery shows that the surface kinetic process controls the microscopic shape. Seemingly, the compact pattern merely appears at the condition at which two mechanisms have an identical contribution.

The formation of the square single crystals indicates that the surface kinetic process completely controls the pattern formation in the temperature range from 53 to 60 °C. This result is similar to those found by Kovacs and co-workers.[41−43] However, we observed that the single crystals of PEO monolayers appear at a temperature lower than those used in their works.

Sample Character. Our literature study shows that the fractal patterns of polymer crystals were found in the polymer blends[28,39] and polymer ultrathin films.[29−34] The samples used in this study were prepared from the dilute solution according to the method detailed in the Experimental Section. Crystalline PEO monolayers with fractal patterns cover only 25−35% of the total surface of the silicon wafer after the solvent was evapored.[34] The thickness of the crystalline layers crystallized at room temperature is 6−7 nm. Clearly, the PEO layer becomes discontinuous after crystallization. In other words, this corresponds to a case that the crystallizable molecules possess a lower "concentration". This is one of important conditions for the fractal pattern formation at nonequilibrium, as presented by a computer simulation.[40] Possibly, this is why such fractal patterns cannot be formed in bulk samples.

Quantized Thickness of PEO Monolayers. Finally, it is worthy to mention that the thickness of PEO crystals decreases in a stepwise manner from 32 nm to about 7 nm with increasing ΔT, as shown in Figure 4. This is a typical feature of such PEO with a lower molecular weight.[35,36] $l \approx 32$ nm (or 0 fold) at $2 \leq \Delta T \leq 7$ °C; $l \approx 16$ nm (or 1 fold) at $8 \leq \Delta T \leq 13$ °C; $l \approx 10.7$ nm (or 2 folds) at $14.5 \leq \Delta T \leq 24$ °C; and $l \approx 7-8$ nm (or 3−4 folds) at $27 \leq \Delta T \leq 37$ °C. The quantized folds are similar those found in bulk samples[35,35] At present, we do not know which role the crystal thickness change plays in the pattern formation.

Conclusion

In summary, the crystal pattern formation and transition of the monolayers of this PEO on the surface of silicon wafer have been studied using atomic force microscopy with a hot stage in the temperature range $25 \leq T_c \leq 60$ °C. Different patterns, like dendrite, seaweed, compact structure, and square single crystals, have been found. The dendrite and seaweed patterns were observed at $25 \leq T_c \leq 49$ °C. They have the same fractal dimension $D_p = 1.672 \pm 0.027$, meaning that the diffusion controlled aggregation is the underlying mechanism. In this temperature range, the dendrite-to-seaweed pattern transition occurs at $T_c = 39.1$ °C. The anisotropic growth causes the dendrite pattern, while the random sticking process results in the seaweed pattern. At $54 \leq T_c \leq 59$ °C the crystals had a square shape and a thickness close to the extended-chain crystals. The surface kinetic process controls the pattern formation. At $49 \leq T_c \leq 53$ °C the governing mechanism implies a turnover. The analysis of fractal dimension shows a gradual loss of fractality. The patterns vary from seaweed to square single crystals in a temperature range of 4 deg, giving rise to high temperature sensitivity. The compact structure merely appears in a very narrow temperature range at which the two mechanisms have an identical contribution.

Acknowledgment. We very greatly appreciate Nankai University for a start-up funding and National Science Foundation of China for a grant (NSFC20474033) to support this work. W.W. thanks the Max-Planck-Institute for Polymer Research (MPI-P) for the determination of molecular weight, for a scholarship, and for a warm hospitalization when he completed this manuscript as a visiting scientist at MPI-P.

References and Notes

(1) Langer, J. S. *Rev. Mod. Phys.* **1980**, *52*, 1.
(2) Meakin, P. *Fractals, Scaling and Growth Far from Equilibrium*; Cambridge University Press: Cambridge, 1997.
(3) Deutscher, G.; Lereah, Y. *Phys. Rev. Lett.* **1988**, *60*, 1510.
(4) Fowler, A. D.; Stanley, H. E.; Daccord, G. *Nature (London)* **1989**, *341*, 134.
(5) Couder, Y.; Argoul, F.; Arnéodo, A.; Maurer, J.; Rabaud, M. *Phys. Rev. A* **1990**, *42*, 3499.
(6) Ben-Jacob, E.; Garik, P. *Nature (London)* **1990**, *343*, 523.
(7) Hwang, R. Q.; Schröder, J.; Günther, C.; Behm, R. *Phys. Rev. Lett.* **1991**, *67*, 3279.
(8) Lereah, Y.; Deutscher, G.; Grünbaum, E. *Phys. Rev. A* **1991**, *44*, 8316.
(9) Lereah, Y.; Zarudi, I.; Grünbaum, E.; Deutscher, G.; Buldyrev, S. V.; Standely, H. E. *Phys. Rev. E* **1994**, *49*, 649.
(10) Reiter, G.; Sommer, J.-U. *Phys. Rev. Lett.* **1998**, *80*, 3771.
(11) Reiter, G.; Sommer, J.-U. *J. Chem. Phys.* **2000**, *112*, 4376.
(12) Utter, B.; Ragnarsson, R.; Bodenschatz, E. *Phys. Rev. Lett.* **2001**, *86*, 4604.
(13) Witten, T. A., Jr.; Sander, L. M. *Phys. Rev. Lett.* **1981**, *47*, 1400; *Phys. Rev. B* **1983**, *27*, 5686.
(14) Meakin, P. *Phys. Rev. A* **1983**, *27*, 604.
(15) Vicsek, T. *Phys. Rev. Lett.* **1984**, *53*, 2281; *Phys. Rev. A* **1985**, *32*, 3084.
(16) Banavar, J. R.; Kohmoto, M.; Roberts, J. *Phys. Rev. A* **1986**, *33*, 2065.
(17) Aukrust, T.; Novotny, M. A,; Browne, D. A.; Kaski, K. *Phys. Rev. A* **1989**, *39*, 2587.
(18) Eckmann, J.-P.; Meakin, P.; Procaccia, I.; Zeitak, R. *Phys. Rev. Lett.* **1990**, *65*, 52.
(19) Yokoyama, E.; Kuroda, T. *Phys. Rev. A* **1990**, *41*, 2038.
(20) Ohta, S.; Honjo, H. *Phys. Rev. A* **1991**, *44*, 8425.
(21) Ihle, T.; Müller-Krumbhaar, H. *Phys. Rev. Lett.* **1993**, *70*, 3083.
(22) Brener, E.; Müller-Krumbhaar, H.; Temkin, D. *Phys. Rev. E* **1996**, *54*, 2714.
(23) Bogoyavlenskiy, V. A.; Chernova, N. A. *Phys. Rev. E* **2000**, *61*, 1629.
(24) Sommer, J.-U.; Reiter, G. *J. Chem. Phys.* **2000**, *112*, 4384.
(25) Wunderlich, B. *Macromolecular Physics;* Academic: New York, 1976; Vols. 1 and 2.
(26) Armistead, K.; Goldbeck-Wood, G. *Adv. Polym. Sci.* **1992**, *100*, 219.
(27) Keller, A.; Cheng, S. Z. D. *Polymer* **1998**, *39*, 4461.
(28) Keith, H. D.; Padden, F. J. *J. Appl. Phys.* **1964**, *35*, 1270.
(29) Lovinger, A. J.; Cais, R. E. *Macromolecules* **1984**, *17*, 1939.
(30) Taguchi, K.; Miyaji, H.; Izumi, K.; Hoshino, A.; Miyamoto, Y.; Kokawa, R. *Polymer* **2001**, *42*, 7443.
(31) Wang, M.; Braun, H. G.; Meyer, E. *Macromolecules* **2004**, *37*, 437.

(32) Gránásy, L.; Pusztai, T.; Börzsönyi, T.; Warren, J. A. *Nat. Mater.* **2004**, *3*, 645.
(33) Mareau, V. H.; Prud'homme, R. E. *Macromolecules* **2005**, *38*, 398.
(34) Zhai, X.-M.; Wang, W.; Ma, Z.-P.; Wen, X.-J.; Yuan, F.; Tang, X.-F.; He, B.-L. *Macromolecules* **2005**, *38*, 1717.
(35) Arlie, P.; Spegt, P. A.; Skoulios, A. *Makomol. Chem.* **1966**, *99*, 160; **1967**, *104*, 212.
(36) Spegt, P. *Makromol. Chem.* **1970**, *139*, 139.
(37) Mandelbrot, B. B. *The Fractal Geometry of Nature;* W.H. Freeman and Co.: San Francisco, 1982. (b) Kaye, B. H. *A Random Walk Through Fractal Dimension;* VCH Publishers: New York, 1989.
(38) Kuroda, T. *Crystals Are Living;* Sa-I-en-su Sha: Tokyo, 1984.
(39) Ferreiro, V.; Douglas, J. F.; Warren, J. A.; Karim, A. *Phys. Rev. E* **2002**, *65*, 051606.
(40) Erlebacher, J.; Searson, P. C.; Sieraski, K. *Phys. Rev. Lett.* **1993**, *71*, 3311.
(41) Kovacs, A.; Gonthier, A.; Straupe, C. *J. Polym. Sci., Polym. Symp.* **1975**, *50*, 283.
(42) Kovacs, A.; Straupe, C.; Gonthier, A. *J. Polym. Sci., Polym. Symp.* **1977**, *59*, 31.
(43) Kovacs, A.; Straupe, C. *Faraday Discuss. Chem. Soc.* **1979**, *68*, 225; *J. Cryst. Growth* **1980**, *48*, 210.

MA051624Y